Stanford Exploration Project, Report SERGEY, November 9, 2000, pages 641–??

Stanford Exploration Project, Report SERGEY, November 9, 2000, pages 641–??

Migration and velocity analysis by velocity continuation

Sergey Fomel[1]

ABSTRACT

Residual and cascaded migration can be described as a continuous process of velocity continuation in the post-migration domain. This process moves reflection events on the migrated seismic sections according to changes in the migration velocity. Understanding the laws of velocity continuation is crucially important for a successful application of migration velocity analysis. In this paper, I derive the kinematic laws for the case of prestack residual migration from simple trigonometric principles. The kinematic laws lead to dynamic theory via the method of characteristics. The main theoretical result is a decomposition of prestack velocity continuation into three different components corresponding to residual normal moveout, residual dip moveout, and residual zero-offset migration. The contribution and properties of each of the three components are analyzed separately.

INTRODUCTION

The conventional approach to the seismic migration theory (Claerbout, 1985; Berkhout, 1985) employs the downward continuation concept. According to this concept, migration extrapolates upgoing reflected waves, recorded on the surface, to the place of their reflection to form an image of subsurface structures. When post-stack migration is performed in the time domain, it possesses peculiar properties, which can lead to a different viewpoint on migration. One of the most interesting properties is an ability to decompose the time migration procedure into a cascade of two or more migrations with smaller migration velocities. This remarkable property is described by Rothman, Levin, and Rocca (1985) as *residual migration*. Larner and Beasley (1987) have generalized the method of residual migration to one of *cascaded migration.* Cascading finite-difference migrations overcomes the dip limitations of conventional finite-difference algorithms (Larner and Beasley, 1987); cascading Stolt-type *f-k* migrations expands their range of validity to the case of a vertically varying velocity (Beasley et al., 1988). Further theoretical generalization sets the number of migrations in a cascade to infinity, making each step in the velocity space infinitely small. This leads to the partial differential equation in the time-midpoint-velocity space, discovered by Claerbout (1986). Claerbout's equation describes the process of *velocity continuation,* which fills the velocity space in the same manner as a set of constant-velocity migrations. Slicing in the migration velocity space

[1]**email:** sergey@sep.stanford.edu

can serve as a method of velocity analysis for migration with nonconstant velocity (Fowler, 1988).

In this paper, I generalize the velocity continuation concept to the case of prestack migration, connecting it with the theory of prestack residual migration (Etgen, 1990). I provide a simplified kinematic derivation of the velocity continuation equation, which is alternative though closely related to the previously published derivations (Claerbout, 1986; Levin, 1986a; Fomel, 1994). Though this derivation is purely kinematic, it leads to differential equations with reasonable dynamic properties. In practice, one can accomplish dynamic velocity continuation by integral, finite-difference, or Fourier-domain methods.

Besides the idea of reviving SEP's results from the epoch of "nonreproducible research," this paper is motivated by the challenge of velocity analysis for prestack 3-D depth migration. Though prestack velocity continuation cannot provide a complete solution to this problem in the areas of lateral velocity variation, it can serve as a useful transformation for simplifying the kinematic features of prestack data and for preconditioning the velocity inversion.

KINEMATICS OF VELOCITY CONTINUATION

From the kinematic point of view, it is convenient to describe the reflector as a locally smooth surface $z = z(x)$, where z is the depth, and x is the point on the surface (x is a two-dimensional vector in the 3-D problem). The image of the reflector obtained after a common-offset prestack migration with a half-offset h and a constant velocity v is the surface $z = z(x;h,v)$. Appendix A provides the derivations of the partial differential equation describing the image surface in the depth-midpoint-offset-velocity space. The purpose of this section is to discuss the laws of kinematic transformations implied by the velocity continuation equation. Later in this paper, I obtain dynamic analogues of the kinematic relationships in order to describe continuation of migrated sections in the velocity space.

The kinematic equation for prestack velocity continuation, derived in Appendix A, takes the following form:

$$\frac{\partial \tau}{\partial v} = v\,\tau \left(\frac{\partial \tau}{\partial x}\right)^2 + \frac{h^2}{v^3\,\tau}\left(1 - v^4 \left(\frac{\partial \tau}{\partial x}\right)^2 \left(\frac{\partial \tau}{\partial h}\right)^2\right). \tag{1}$$

Here τ denotes the one-way vertical traveltime $\left(\tau = \frac{z}{v}\right)$. The right-hand side of equation (1) consists of three distinctive terms. Each has its own geophysical meaning. The first term is the only one remaining when the offset h equals zero. It corresponds to the procedure of *zero-offset residual migration*. Setting the reflector dip to zero eliminates the first and third terms, leaving the second, dip-independent one. We can associate the second term with the process of *residual normal moveout*. The third term is both dip- and offset- dependent. The process that it describes is *residual dip moveout*. It is convenient to analyze each of the three processes separately, evaluating their contributions to the cumulative process of prestack velocity continuation.

Kinematics of Zero-Offset Velocity Continuation

The kinematic equation for zero-offset velocity continuation is

$$\frac{\partial \tau}{\partial v} = v\,\tau \left(\frac{\partial \tau}{\partial x}\right)^2 . \tag{2}$$

The typical boundary problem associated with it is to find the traveltime surface $\tau(x)$ for a constant velocity v, given the traveltime surface $\tau_1(x_1)$ at some other velocity v_1. Both surfaces correspond to the reflector images obtained by time migrations with the specified velocities. When the migration velocity approaches zero, post-stack time migration approaches the identity operator. Therefore, the case of $v_1 = 0$ corresponds kinematically to the zero-offset (post-stack) migration, and the case of $v = 0$ corresponds to the zero-offset modeling (demigration).

The appropriate mathematical method of solving the kinematic problem posed above is the method of characteristics (Courant, 1962). The characteristics of equation (2) are the trajectories followed by individual points of the reflector image in the velocity continuation process, which I have called *velocity rays* (Fomel, 1994). Velocity rays are defined by the system of ordinary differential equations derived from (2) according to the classic rules of mathematical physics:

$$\frac{dx}{dv} = -2\,v\,\tau\,\tau_x \quad , \quad \frac{d\tau}{dv} = -\tau_v \, , \tag{3}$$

$$\frac{d\tau_x}{dv} = v\,\tau_x^3 \quad , \quad \frac{d\tau_v}{dv} = (\tau + v\,\tau_v)\,\tau_x^2 \, . \tag{4}$$

An additional constraint for the quantities τ_x and τ_v follows from equation (2), rewritten in the form

$$\tau_v = v\,\tau\,\tau_x^2 \, . \tag{5}$$

One can easily solve the system of equations (3) and (4) by the classic mathematical methods for the ordinary differential equations. The general solution of the system takes the parametric form

$$x(v) = A - C v^2 \, , \; \tau^2(v) = B - C^2 v^2 \, , \tag{6}$$

$$\tau_x(v) = \frac{C}{\tau(v)} \, , \; \tau_v(v) = \frac{C^2 v}{\tau(v)} \, , \tag{7}$$

where A, B, and C are constant along each individual velocity ray. These three constants are determined from the boundary conditions as

$$A = x_1 + v_1^2\,\tau_1 \frac{\partial \tau_1}{\partial x_1} = x_0 \, , \tag{8}$$

$$B = \tau_1^2 \left(1 + v^2 \left(\frac{\partial \tau_1}{\partial x_1}\right)^2\right) = \tau_0^2 \, , \tag{9}$$

$$C = \tau_1 \frac{\partial \tau_1}{\partial x_1} = \tau_0 \frac{\partial \tau_0}{\partial x_0} \,, \tag{10}$$

where τ_0 and x_0 correspond to the zero velocity (unmigrated section). Equations (8), (9), and (10) have a clear geometric meaning illustrated in Figure 1. Noting the simple relationship between the midpoint derivative of the vertical traveltime and the local dip angle α (appendix A),

$$\frac{\partial \tau}{\partial x} = \frac{\tan\alpha}{v} \,, \tag{11}$$

we can see that equations (8) and (9) are precisely equivalent to the evident geometric relationships

$$x + v\,\tau\,\tan\alpha = x_0 \,, \quad \frac{\tau}{\cos\alpha} = \tau_0 \,. \tag{12}$$

Equation (10) states that the points on a velocity ray correspond to a single reflection point, constrained by the values of τ, v, and α. As follows from equations (6), the projection of a velocity ray to the time-midpoint plane has the parabolic shape $x(\tau) = A + (\tau^2 - B)/C$, which has been noticed by Chun and Jacewitz (1981). On the depth-midpoint plane, the velocity rays have the circular shape $z^2(x) = (A-x)\,B/C - (A-x)^2$, described by Liptow and Hubral (1995) as "Thales circles."

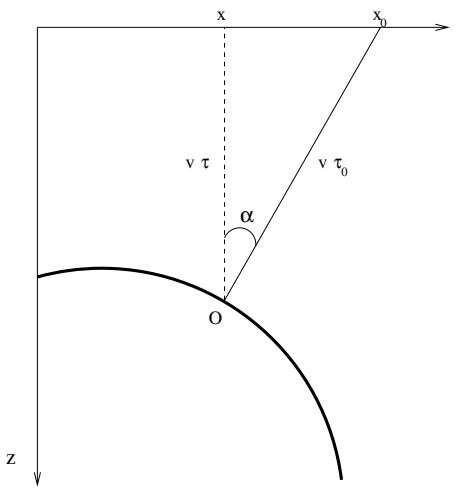

Figure 1: Zero-offset reflection in a constant velocity medium (a scheme). velcon1-vlczor [NR]

For an example of kinematic continuation by velocity rays, let us consider the case of a point diffractor. If the diffractor location in the subsurface is the point x_d, z_d, then the reflection traveltime at zero offset is defined from Pythagoras's theorem as the hyperbolic curve

$$\tau_0(x_0) = \frac{\sqrt{z_d^2 + (x_0 - x_d)^2}}{v_d} \,, \tag{13}$$

where v is half of the actual velocity. Applying formulas (6), we can deduce that the velocity

rays in this case have the following mathematical expressions:

$$x(v) = x_d \frac{v^2}{v_d^2} + x_0 \left(1 - \frac{v^2}{v_d^2}\right) , \tag{14}$$

$$\tau^2(v) = \tau_d^2 + \frac{(x_0 - x_d)^2}{v_d^2} \left(1 - \frac{v^2}{v_d^2}\right) , \tag{15}$$

where $\tau_d = \frac{z_d}{v_d}$. Eliminating x_0 from the system of equations (14) and (15) leads to the expression for the velocity continuation "wavefront":

$$\tau(x) = \sqrt{\tau_d^2 + \frac{(x - x_d)^2}{v_d^2 - v^2}} . \tag{16}$$

For the case of a point diffractor, the wavefront corresponds precisely to the summation path of the residual migration operator (Rothman et al., 1985). It has a hyperbolic shape when $v_d > v$ (undermigration) and an elliptic shape when $v_d < v$ (overmigration). The wavefront collapses to a point when the velocity v coincides with the actual effective velocity v_d. At zero velocity, $v = 0$, the wavefront takes the familiar form of the post-stack migration hyperbolic summation path. The form of the velocity rays and wavefronts is illustrated in the left plot of Figure 2.

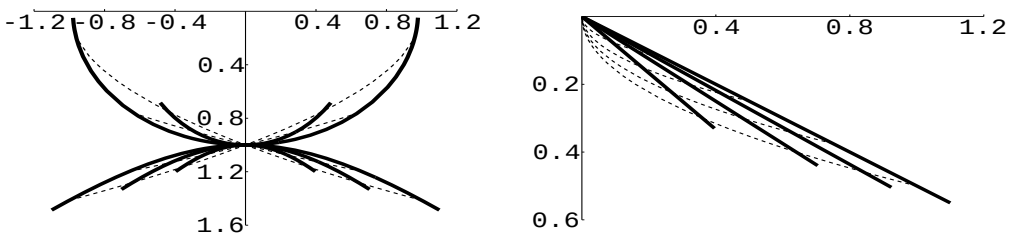

Figure 2: Kinematic velocity continuation in the post-stack migration domain. Solid lines denote wavefronts: reflector images for different migration velocities; dashed lines denote velocity rays. Left: the case of a point diffractor. Right: the case of a dipping plane reflector. velcon1-vlcvrs [CR]

Another important example is the case of a dipping plane reflector. For simplicity, let us put the origin of the midpoint coordinate x at the point of the plane intersection with the surface of observations. In this case, the plane reflector has the simple expression

$$z_p(x) = x \tan\alpha , \tag{17}$$

where α is the dip angle. The zero-offset reflection traveltime is the plane with a changed angle. It can be expressed as

$$\tau_0(x_0) = p\, x_0 , \tag{18}$$

where $p = \frac{\sin\alpha}{v_p}$, and v_p is the half of the actual velocity. Applying formulas (6) leads to the following parametric expression for the velocity rays:

$$x(v) = x_0 (1 - p^2 v^2) , \tag{19}$$
$$\tau(v) = p\, x_0 \sqrt{1 - p^2 v^2} . \tag{20}$$

Eliminating x_0 from the system of equations (19) and (20) shows that the velocity continuation wavefronts are planes with a modified angle:

$$\tau(x) = \frac{p\, x}{\sqrt{1 - p^2 v^2}} . \tag{21}$$

The right plot of Figure 2 shows the geometry of the kinematic velocity continuation for the case of a plane reflector.

Kinematics of Residual NMO

The residual NMO differential equation is the second term in (1):

$$\frac{\partial \tau}{\partial v} = \frac{h^2}{v^3 \tau} . \tag{22}$$

Equation (22) is independent from the midpoint x. This fact indicates the one-dimensional nature of normal moveout. The general solution of equation (22) is obtained by simple integration. It takes the form

$$\tau^2(v) = C - \frac{h^2}{v^2} = \tau_1^2 + h^2 \left(\frac{1}{v_1^2} - \frac{1}{v^2} \right) , \tag{23}$$

where C is an arbitrary velocity-independent constant, and I have chosen the constants τ_1 and v_1 so that $\tau(v_1) = \tau_1$.

For the case of a point diffractor, solution (23) easily combines with the zero-offset solution (16). The result is a simplified version of the prestack residual migration summation path:

$$\tau(x) = \sqrt{\tau_d^2 + \frac{(x - x_d)^2}{v_d^2 - v^2} + h^2 \left(\frac{1}{v_d^2} - \frac{1}{v^2} \right)} . \tag{24}$$

Summation paths of the form (24) for a set of diffractors with different depths are plotted in Figures 3 and 4. The parameters chosen in these plots allow a direct comparison with Etgen's Figures 2.4 and 2.5 (Etgen, 1990), based on the exact solution and reproduced in Figures 9 and 10. The comparison shows that the approximate solution (24) captures the main features of the prestack residual migration operator, except for the residual DMO cusps appearing in the exact solution when the diffractor depth is smaller than the offset.

Neglecting the residual DMO term in residual migration is approximately equivalent in accuracy to neglecting the DMO step in conventional processing. Indeed, as follows from the

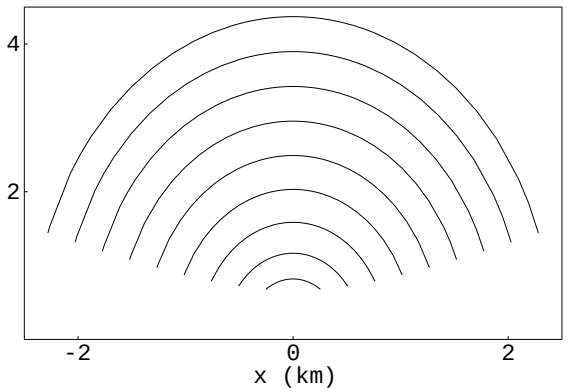

Figure 3: Summation paths of the simplified prestack residual migration for a series of depth diffractors. Residual slowness v/v_d is 1.2; offset h is 1 km. This figure is to be compared with Etgen's Figure 2.4. velcon1-vlcve1 [CR]

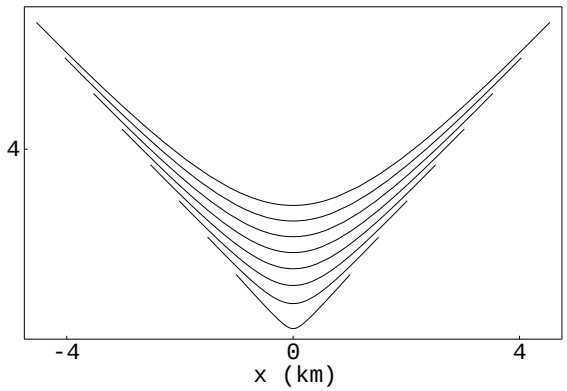

Figure 4: Summation paths of the simplified prestack residual migration for a series of depth diffractors. Residual slowness v/v_d is 0.8; offset h is 1 km. This figure is to be compared with Etgen's Figure 2.5. velcon1-vlcve2 [CR]

geometric analogue of equation (1) derived in Appendix A, dropping the residual DMO term corresponds to the condition

$$\tan^2\alpha \tan^2\gamma \ll 1 \,, \tag{25}$$

where α is the dip angle, and γ is the reflection angle. As shown by Yilmaz and Claerbout (1980), the conventional processing sequence without the DMO step corresponds to the separable approximation of the double-square-root equation (A-4):

$$\sqrt{1-v^2\left(\frac{\partial t}{\partial s}\right)^2}+\sqrt{1-v^2\left(\frac{\partial t}{\partial r}\right)^2}\approx 2\sqrt{1-v^2\left(\frac{\partial t}{\partial x}\right)^2}+2\sqrt{1-v^2\left(\frac{\partial t}{\partial h}\right)^2}-2\,. \tag{26}$$

In geometric terms, approximation (26) transforms to

$$\cos\alpha\cos\gamma \approx \sqrt{1-\sin^2\alpha\cos^2\gamma}+\sqrt{1-\sin^2\gamma\cos^2\alpha}-1\,. \tag{27}$$

Estimating the accuracy of the separable approximation by the first term of the Taylor series for small α and γ yields the estimate of $\frac{3}{4}\tan^2\alpha\tan^2\gamma$ (Yilmaz and Claerbout, 1980), which agrees qualitatively with (25). Though approximation (24) fails in situations where the dip moveout correction is necessary, it is significantly more accurate than the 15-degree approximation of the double-square-root equation, implied in the migration velocity analysis method of Yilmaz and Chambers (1984) and MacKay and Abma (1992). The 15-degree approxima-

tion

$$\sqrt{1-v^2\left(\frac{\partial t}{\partial s}\right)^2}+\sqrt{1-v^2\left(\frac{\partial t}{\partial r}\right)^2}\approx 2-\frac{v^2}{2}\left(\left(\frac{\partial t}{\partial s}\right)^2+\left(\frac{\partial t}{\partial s}\right)^2\right) \tag{28}$$

corresponds geometrically to the equation

$$2\cos\alpha\cos\gamma\approx\frac{3+\cos 2\alpha\cos 2\gamma}{2}\,. \tag{29}$$

Its estimated accuracy is $\frac{1}{8}\tan^2\alpha+\frac{1}{8}\tan^2\gamma$. Unlike the separable approximation, which is accurate separately for zero offset and zero dip, the 15-degree approximation fails at zero offset in the case of a steep dip and at zero dip in the case of a large offset.

Kinematics of Residual DMO

The partial differential equation for kinematic residual DMO is the third term in (1):

$$\frac{\partial\tau}{\partial v}=-\frac{h^2 v}{\tau}\left(\frac{\partial\tau}{\partial x}\right)^2\left(\frac{\partial\tau}{\partial h}\right)^2\,. \tag{30}$$

It is more convenient to consider the residual dip-moveout process coupled with residual normal moveout. Etgen (1990) describes this procedure as the cascade of inverse DMO with the initial velocity v_0, residual NMO, and DMO with the updated velocity v_1. The kinematic equation for residual NMO+DMO is the sum of the two terms in (1):

$$\frac{\partial\tau}{\partial v}=\frac{h^2}{v^3\tau}\left(1-v^4\left(\frac{\partial\tau}{\partial x}\right)^2\left(\frac{\partial\tau}{\partial h}\right)^2\right)\,. \tag{31}$$

If the boundary data for equation (31) are on a common-offset gather, it is appropriate to rewrite this equation purely in terms of the midpoint derivative $\frac{\partial\tau}{\partial x}$, eliminating the offset-derivative term $\frac{\partial\tau}{\partial h}$. The resultant expression, derived in Appendix A, has the form

$$v^3\frac{\partial\tau}{\partial v}=\frac{2h^2}{\sqrt{\tau^2+4h^2\,Q\left(v,\frac{\partial\tau}{\partial x}\right)}+\tau}\,, \tag{32}$$

where

$$Q(v,\tau_x)=\frac{\tau_x^2}{\left(1+v^2\tau_x^2\right)^2}\,. \tag{33}$$

The direct solution of equation (32) is nontrivial. A simpler way to obtain this solution is to decompose residual NMO+DMO into three steps and to evaluate their contributions separately. Let the initial data be the zero-offset reflection event $\tau_0(x_0)$. The first step of the residual NMO+DMO is the inverse DMO operator. One can evaluate the effect of this operator by means of the offset continuation concept (Fomel, 1995). According to this concept, each point

of the input traveltime curve $\tau_0(x_0)$ travels with the change of the offset from zero to h along a special trajectory, which I call a *time ray*. Time rays are parabolic curves of the form

$$x(\tau) = x_0 + \frac{\tau^2 - \tau_0^2(x_0)}{\tau_0(x_0)\,\tau_0'(x_0)}\,, \tag{34}$$

with the final points constrained by the equation

$$h^2 = \tau^2\,\frac{\tau^2 - \tau_0^2(x_0)}{\left(\tau_0(x_0)\,\tau_0'(x_0)\right)^2}\,. \tag{35}$$

The second step of the cumulative residual NMO+DMO process is the residual normal moveout. According to equation (23), residual NMO is a one-trace operation transforming the traveltime τ to τ_1 as follows:

$$\tau_1^2 = \tau^2 + h^2\,s\,, \tag{36}$$

where

$$s = \frac{1}{v_0^2} - \frac{1}{v_1^2}\,. \tag{37}$$

The third step is dip moveout corresponding to the new velocity v_1. DMO is the offset continuation from h to zero offset along the redefined time rays (Fomel, 1995)

$$x_2(\tau_2) = x + \frac{h\,X}{\tau_1^2\,H}\left(\tau_1^2 - \tau_2^2\right)\,, \tag{38}$$

where $H = \frac{\partial \tau_1}{\partial h}$, and $X = \frac{\partial \tau_1}{\partial x}$. The end points of the time rays (38) are defined by the equation

$$\tau_2^2 = -\tau_1^2\,\frac{\tau_1\,H}{h\,X^2}\,. \tag{39}$$

The partial derivatives of the common-offset traveltimes are constrained by the offset continuation kinematic equation

$$h\,(H^2 - Y^2) = \tau_1\,H\,, \tag{40}$$

which is equivalent to equation (A-12) in Appendix A. Additionally, as follows from equations (36) and the ray invariant equations from (Fomel, 1995),

$$\tau_1\,X = \tau\,\frac{\partial \tau}{\partial x} = \frac{\tau^2\,\tau_0'(x_0)}{\tau_0(x_0)}\,. \tag{41}$$

Substituting (34), (35), (36), (40), and (41) into equations (38) and (39) and performing the algebraic simplifications, we arrive at the parametric expressions for velocity rays of the residual NMO+DMO process:

$$\left\{\begin{array}{rcl} x_2(s) &=& x_0 + \dfrac{h^2\,\tau_0'(x_0)}{T}\left(1 - \dfrac{T^2}{T_2^2(s)}\right)\,, \\ \\ \tau(s) &=& \dfrac{\tau_1^2(s)}{T_2(s)}\,, \end{array}\right. \tag{42}$$

where the function $T\left(h,\tau_0(x_0),\tau_0'(x_0)\right)$ is defined by

$$T\left(h,\tau,\tau_x\right)=\frac{\tau+\sqrt{\tau^2+4h^2\,\tau_x^2}}{2}\,, \tag{43}$$

$$T_2(s)=\sqrt{T\left(h,\tau_1^2(s),\tau_0'(x_0)\;T\left(h,\tau_0(x_0),\tau_0'(x_0)\right)\right)}\,, \tag{44}$$

and

$$\tau_1^2(s)=\tau_0\,T+s\,h^2\,. \tag{45}$$

The last step of the cascade of inverse DMO, residual NMO, and DMO is illustrated in Figure 5. The three plots in the figure show the offset continuation to zero offset of the inverse DMO impulse response shifted by the residual NMO operator. The middle plot corresponds to zero NMO shift, for which the DMO step collapses the wavefront back to a point. Both positive (top plot) and negative (bottom plot) NMO shifts result in the formation of the specific triangular impulse response of the residual NMO+DMO operator. As noticed by Etgen (1990), the size of the "triangle" operators dramatically decreases with the time increase. For large times (pseudo-depths) of the initial impulses, the operator collapses to a point corresponding to the pure NMO shift. This fact agrees with the conclusions of the preceding subsection about the comparative importance of the residual DMO term. It is illustrated in Figure 6 with the theoretical impulse response curves, and in Figure 7 with the result of an actual cascade of the inverse DMO, residual NMO, and DMO operators.

Figure 8 illustrates the residual NMO+DMO velocity continuation for two particularly interesting cases. The left plot shows the continuation for a point diffractor. One can see that when the velocity error is large, focusing of the velocity rays forms a specific loop on the zero-offset hyperbola. The right plot illustrates the case of a plane dipping reflector. The image of the reflector shifts both vertically and laterally with the change in NMO velocity.

The full residual migration operator is the result of cascading residual zero-offset migration and residual NMO+DMO. I illustrate the kinematics of this operator in Figures 9 and 10, which are designed to match Etgen's Figures 2.4 and 2.5 (Etgen, 1990). A comparison with Figures 3 and 4 shows that including the residual DMO term affects the images of shallow objects (with the depth smaller than the offset h) and complicates the residual migration operator with cusps.

FROM KINEMATICS TO DYNAMICS

The theory of characteristics (Courant, 1962) states that if a partial differential equation has the form

$$\sum_{i,j=1}^{n}\Lambda_{ij}(\xi_1,\ldots,\xi_n)\,\frac{\partial^2 P}{\partial\xi_i\,\partial\xi_j}+F\left(\xi_1,\ldots,\xi_n,P,\frac{\partial P}{\partial\xi_1},\ldots,\frac{\partial P}{\partial\xi_n}\right)=0\,, \tag{46}$$

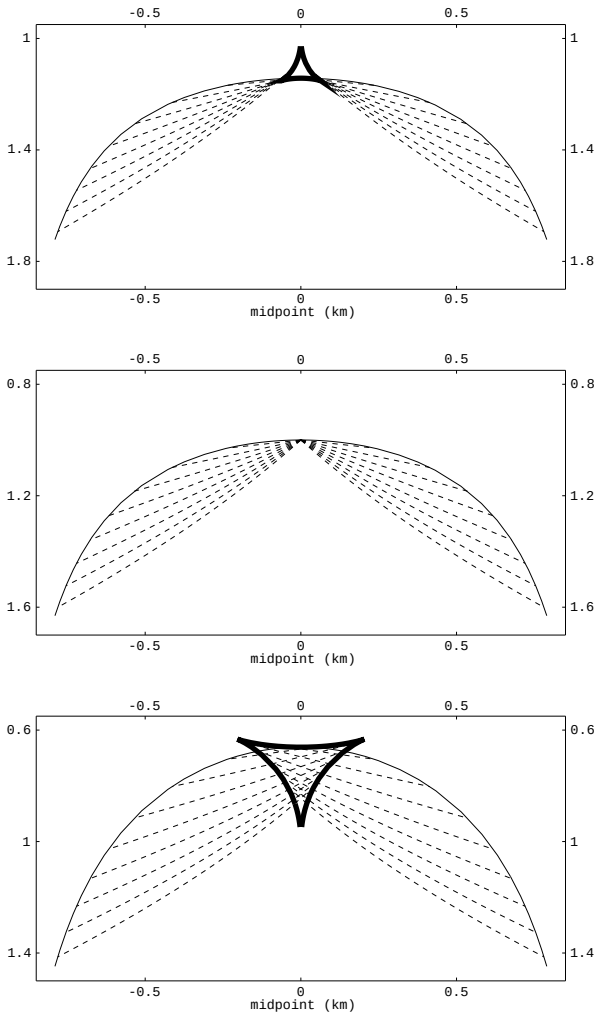

Figure 5: Kinematic residual NMO+DMO operators constructed by the cascade of inverse DMO, residual NMO, and DMO. The impulse response of inverse DMO is shifted by the residual DMO procedure. Offset continuation back to zero offset forms the impulse response of the residual NMO+DMO operator. Solid lines denote travel-time curves; dashed lines denote the offset continuation trajectories (time rays). Top plot: $v_1/v_0 = 1.2$. Middle plot: $v_1/v_0 = 1$; the inverse DMO impulse response collapses back to the initial impulse. Bottom plot: $v_1/v_0 = 0.8$. The half-offset h in all three plots is 1 km. velcon1-vlcvoc [CR]

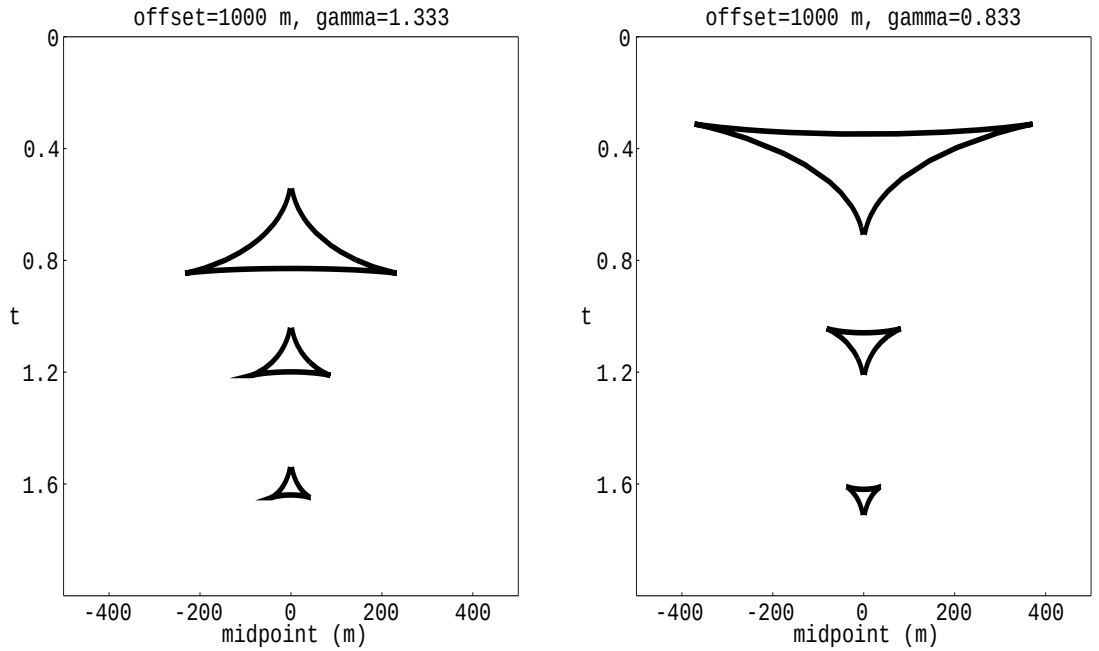

Figure 6: Theoretical kinematics of the residual NMO+DMO impulse responses for three impulses. Left plot: the velocity ratio v_1/v_0 is 1.333. Right plot: the velocity ratio v_1/v_0 is 0.833. In both cases the half-offset h is 1 km. velcon1-vlcvcp [CR]

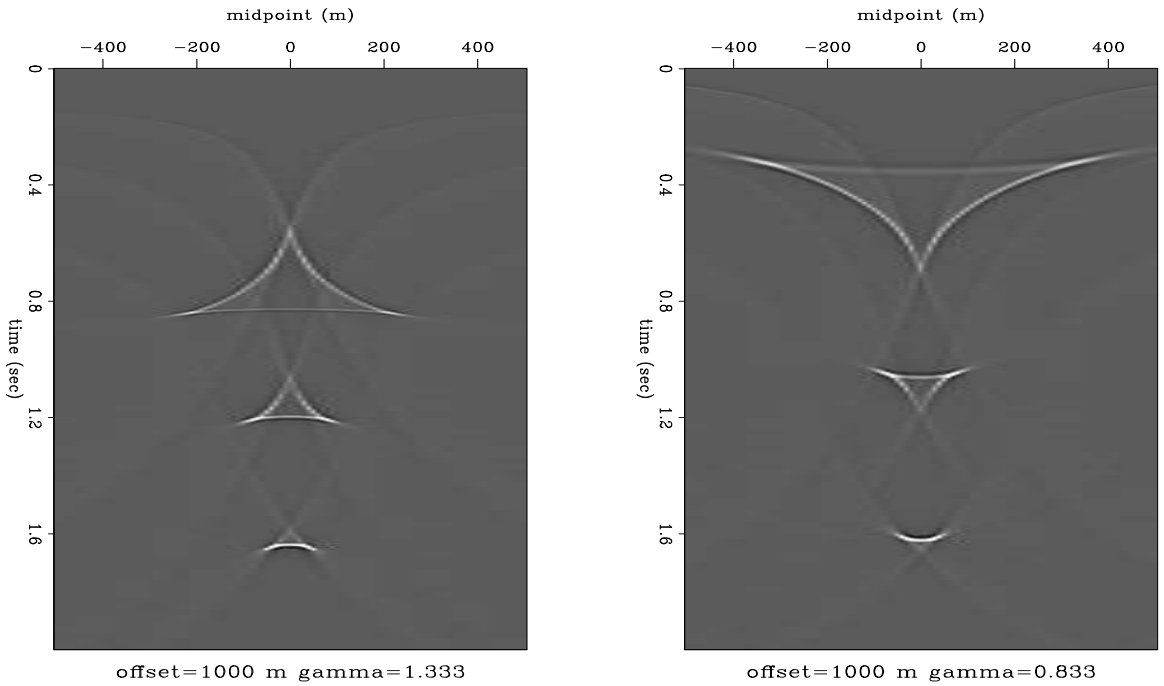

Figure 7: The result of residual NMO+DMO (cascading inverse DMO, residual NMO, and DMO) for three impulses. Left plot: the velocity ratio v_1/v_0 is 1.333. Right plot: the velocity ratio v_1/v_0 is 0.833. In both cases the half-offset h is 1 km. velcon1-vlccps [ER]

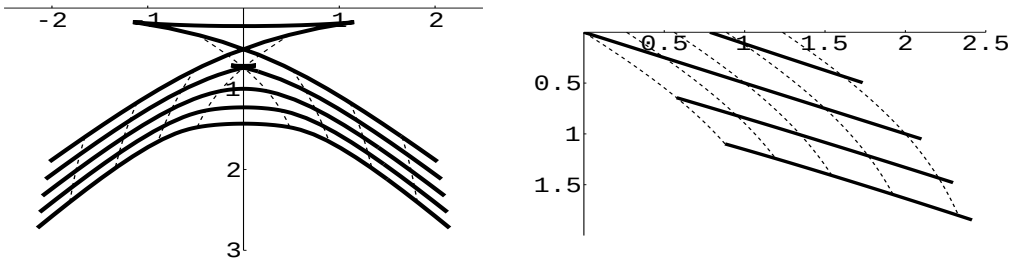

Figure 8: Kinematic velocity continuation for residual NMO+DMO. Solid lines denote wavefronts: zero-offset traveltime curves; dashed lines denote velocity rays. Left plot: the case of a point diffractor; the velocity ratio v_1/v_0 changes from 0.9 to 1.1. Right plot: the case of a dipping plane reflector; the velocity ratio v_1/v_0 changes from 0.8 to 1.2. In both cases, the half-offset h is 2 km. velcon1-vlcvrd [CR]

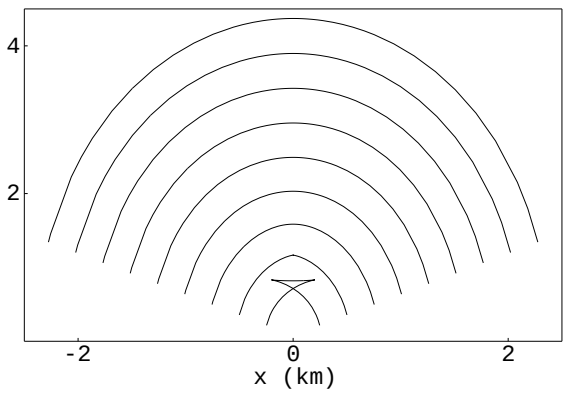

Figure 9: Summation paths of prestack residual migration for a series of depth diffractors. Residual slowness v/v_d is 1.2; offset h is 1 km. This figure reproduces Etgen's Figure 2.4. velcon1-vlcve3 [CR]

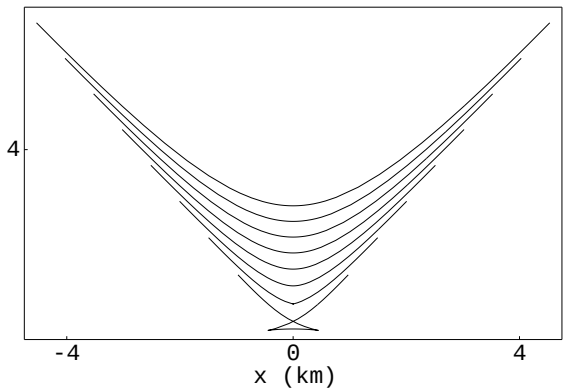

Figure 10: Summation paths of prestack residual migration for a series of depth diffractors. Residual slowness v/v_d is 0.8; offset h is 1 km. This figure reproduces Etgen's Figure 2.5. velcon1-vlcve4 [CR]

where F is some arbitrary function, and if the eigenvalues of the matrix Λ are nonzero, and one of them is different in sign from the others, then equation (46) describes a wave-type process, and its kinematic counterpart is the characteristic equation

$$\sum_{i,j=1}^{n} \Lambda_{ij}(\xi_1,\ldots,\xi_n)\frac{\partial \psi}{\partial \xi_i}\frac{\partial \psi}{\partial \xi_j} = 0 \tag{47}$$

with the characteristic surface

$$\psi(\xi_1,\ldots,\xi_n) = 0 \tag{48}$$

corresponding to the wavefront. In velocity continuation problems, it is appropriate to choose the variable ξ_1 to denote the time t, ξ_2 to denote the velocity v, and the rest of the ξ-variables to denote one or two lateral coordinates x. Without loss of generality, we can set the characteristic surface to be

$$\psi = t - \tau(x;v) = 0\,, \tag{49}$$

and use the theory of characteristics to reconstruct the main (second-order) part of the dynamic differential equation from the corresponding kinematic equations. As in the preceding section, it is convenient to consider separately the three different components of the prestack velocity continuation process.

Dynamics of Zero-Offset Velocity Continuation

In the case of zero-offset velocity continuation, the characteristic equation is reconstructed from equation (2) to have the form

$$\frac{\partial \psi}{\partial v}\frac{\partial \psi}{\partial t} + v\,t\left(\frac{\partial \psi}{\partial x}\right)^2 = 0\,. \tag{50}$$

According to formula (46), the corresponding dynamic equation is

$$\frac{\partial^2 P}{\partial v\,\partial t} + v\,t\,\frac{\partial^2 P}{\partial x^2} + F\left(x,t,v,P,\frac{\partial P}{\partial t},\frac{\partial P}{\partial v},\frac{\partial P}{\partial x}\right) = 0\,, \tag{51}$$

where the function F remains to be defined. The simplest case of F equal to zero corresponds to Claerbout's velocity continuation equation (Claerbout, 1986), derived in a different way. Levin (1986a) provides the dispersion-relation derivation, conceptually analogous to applying the method of characteristics.

In high-frequency asymptotics, the wavefield P can be represented by the ray-theoretical (WKBJ) approximation,

$$P(t,x,v) \approx A(x,v)\,f\left(t-\tau(x,v)\right)\,, \tag{52}$$

where A is the amplitude, f is the short (high-frequency) wavelet, and the function τ satisfies the kinematic equation (2). Substituting approximation (52) into the dynamic velocity continuation equation (51), collecting the leading-order terms, and neglecting the F function, we arrive at the partial differential equation for amplitude transport:

$$\frac{\partial A}{\partial v} = v\,\tau\left(2\,\frac{\partial A}{\partial x}\,\frac{\partial \tau}{\partial x} + A\,\frac{\partial^2 \tau}{\partial x^2}\right). \tag{53}$$

The general solution of equation (53) follows from the theory of characteristics. It takes the form

$$A(x,v) = A_0(x_0)\exp\left(\int_0^v u\,\tau(x,u)\,\frac{\partial^2 \tau(x,u)}{\partial x^2}\,du\right), \tag{54}$$

where $A_0(x_0) = A(x,0)$, and the integral corresponds to the curvilinear integration along the corresponding velocity ray. In the case of a plane dipping reflector, the image of the reflector remains plane in the velocity continuation process. Therefore, the second traveltime derivative $\frac{\partial^2 \tau(x,u)}{\partial x^2}$ in (54) equals zero, and the exponential is equal to one. This means that the amplitude of the image doesn't change with the velocity along the velocity rays. This fact doesn't agree with the theory of conventional post-stack migration, which suggests downscaling the image by the "cosine" factor $\frac{\tau_0}{\tau}$ (Chun and Jacewitz, 1981; Levin, 1986b). The simplest way to include the cosine factor in the velocity continuation equation is to set the function F to be $\frac{1}{t}\,\frac{\partial P}{\partial v}$. The resulting differential equation

$$\frac{\partial^2 P}{\partial v\,\partial t} + v\,t\,\frac{\partial^2 P}{\partial x^2} + \frac{1}{t}\,\frac{\partial P}{\partial v} = 0 \tag{55}$$

has the amplitude transport

$$A(x,v) = \frac{\tau_0}{\tau}\,A_0(x_0)\exp\left(\int_0^v u\,\tau(x,u)\,\frac{\partial^2 \tau(x,u)}{\partial x^2}\,du\right), \tag{56}$$

corresponding to the differential equation

$$\frac{\partial A}{\partial v} = v\,\tau\left(2\,\frac{\partial A}{\partial x}\,\frac{\partial \tau}{\partial x} + A\,\frac{\partial^2 \tau}{\partial x^2}\right) - A\,\frac{1}{\tau}\,\frac{\partial \tau}{\partial v}. \tag{57}$$

Appendix B proves that the time-and-space solution of the dynamic velocity continuation equation (55) coincides with the conventional Kirchhoff migration operator.

The finite-difference implementation of zero-offset velocity continuation resembles the implementation of Claerbout's 15-degree equation in a retarded coordinate system (Claerbout, 1976). This implementation is discussed in more detail in Appendix C.

Dynamics of Residual NMO

According to the theory of characteristics, described in the beginning of this section, the kinematic residual NMO equation (22) corresponds to the dynamic equation of the form

$$\frac{\partial P}{\partial v} + \frac{h^2}{v^3\,t}\,\frac{\partial P}{\partial t}, \tag{58}$$

whose general solution is easily found to be

$$P(t,x,v) = \phi\left(t^2 + \frac{h^2}{v^2}\right) , \tag{59}$$

where ϕ is an arbitrary smooth function. The combination of dynamic equations (58) and (55) leads to an approximate prestack velocity continuation with the residual DMO effect neglected. To accomplish the combination, we can simply add the term $\frac{h^2}{v^3 t}\frac{\partial^2 P}{\partial t^2}$ to the left-hand side of equation (55). This addition changes the kinematics of velocity continuation, but doesn't change the amplitude properties embedded in the transport equation (56).

Dynamics of Residual DMO

The case of residual DMO complicates building of a dynamic equation because of the essential nonlinearity of the kinematic equation (32). One possible way to linearize the problem is to increase the order of the equation. In this case, the resultant dynamic equation would include a term with the second-order derivative with respect to velocity v. Such an equation describes two different modes of wave propagation and requires additional initial conditions to separate them. Another possible way to linearize equation (32) is to approximate it at small dip angles. For example, one can obtain a recursively accurate approximation by a continuous fraction expansion of the square root in equation (32), analogously to Muir's method in conventional finite-difference migration (Claerbout, 1985). In this case, the dynamic equation would contain only the first-order derivative with respect to the velocity and high-order derivatives with respect to other parameters. The third, and probably the most attractive, method is to change the domain of consideration. For example, we could switch from the common-offset domain to the domain of common offset dip. This method implies a transformation similar to slant stacking of common-midpoint gathers in the post-migration domain in order to obtain the local offset dip information. Equation (32) transforms, with the help of the results from Appendix A, to the form

$$v^3 \frac{\partial \tau}{\partial v} = \frac{\tau \sin^2\gamma}{\cos^2\alpha - \sin^2\gamma} , \tag{60}$$

with

$$\cos^2\alpha = \left(1 + v^2\left(\frac{\partial \tau}{\partial x}\right)^2\right)^{-1} , \tag{61}$$

and

$$\sin^2\alpha = v^2\left(\frac{\partial \tau}{\partial h}\right)^2\left(1 + v^2\left(\frac{\partial \tau}{\partial h}\right)^2\right)^{-1} . \tag{62}$$

For a constant offset dip $\tan\gamma = v\frac{\partial \tau}{\partial h}$, the dynamic analogue of equation (60) is the third-order partial differential equation

$$v\cot^2\gamma\,\frac{\partial^3 P}{\partial t^2\,\partial v} - v^3\frac{\partial^3 P}{\partial x^2\,\partial v} + t\,\frac{\partial^3 P}{\partial t^2\,\partial v} + v^2 t\,\frac{\partial^3 P}{\partial x^2\,\partial t} = 0 . \tag{63}$$

Equation (63) doesn't strictly comply with the theory of second-order linear differential equations. Its properties and practical applicability require further research.

CONCLUSIONS

I have derived kinematic and dynamic equations for residual time migration in the form of a continuous velocity continuation process. This derivation explicitly decomposes prestack velocity continuation into three parts corresponding to zero-offset continuation, residual NMO, and residual DMO. These three parts can be treated separately both for simplicity of theoretical analysis and for practical purposes. It is important to note that in the case of a three-dimensional migration, all three components of velocity continuation have different dimensionality. Zero-offset continuation is fully 3-D. It can be split into two 2-D continuations in the in- and cross-line directions. Residual DMO is a two-dimensional common-azimuth process. Residual NMO is a 1-D single-trace procedure.

The dynamic properties of zero-offset velocity continuation are precisely equivalent to the dynamic properties of conventional post-stack migration methods such as Kirchhoff migration. Moreover, the Kirchhoff migration operator coincides with the integral solution of the velocity continuation differential equation for continuation from the zero velocity plane.

This rigorous theory of velocity continuation can give us new insights into the methods of prestack migration velocity analysis. However, its practical applicability faces several important problems. One of them concerns the comparative value of the residual DMO term. Another problem is the choice of the implementation method for velocity continuation. Both these problems require further research efforts.

ACKNOWLEDGMENTS

I thank Jon Claerbout for his interest in this project and for sharing his old finite-difference codes. I would also like to thank Sergey Goldin, Biondo Biondi, Bill Harlan, and David Lumley for encouraging discussions about the velocity continuation concept.

REFERENCES

Beasley, C., Lynn, W., Larner, K., and Nguyen, H., 1988, Cascaded frequency-wavenumber migration—Removing the restrictions on depth-varying velocity: Geophysics, **53**, no. 7, 881–893.

Belonosova, A. V., and Alekseev, A. S., 1967, About one formulation of the inverse kinematic problem of seismics for a two-dimensional continuously heterogeneous medium:, *in* Some methods and algorithms for interpretation of geophysical data (in Russian) Nauka, 137–154.

Berkhout, A. J., 1985, Seismic migration: Imaging of acoustic energy by wave field extrapolation: Elsevier, Amsterdam.

Chun, J. H., and Jacewitz, C. A., 1981, Fundamentals of frequency-domain migration: Geophysics, **46**, no. 5, 717–733.

Claerbout, J. F., 1976, Fundamentals of geophysical data processing: Blackwell.

Claerbout, J. F., 1985, Imaging the Earth's Interior: Blackwell Scientific Publications.

Claerbout, J. F., 1986, Velocity extrapolation by cascaded 15 degree migration: SEP–**48**, 79–84.

Claerbout, J. F., 1995, Basic Earth Imaging: Stanford Exploration Project.

Clayton, R. W., 1978, Common midpoint migration: SEP–**14**, 21–36.

Courant, R., 1962, Methods of mathematical physics: Interscience Publishers, New York.

Etgen, J., 1990, Residual prestack migration and interval velocity estimation: Ph.D. thesis, Stanford University.

Fomel, S., and Biondi, B., 1995, Azimuth moveout: the operator parameterization and antialiasing: SEP–**89**, 89–108.

Fomel, S. B., 1994, Method of velocity continuation in the problem of temporal seismic migration: Russian Geology and Geophysics, **35**, no. 5, 100–111.

Fomel, S., 1995, Amplitude preserving offset continuation in theory Part 1: The offset continuation equation: SEP–**84**, 179–198.

Fomel, S., 1996, Stacking operators: Adjoint versus asymptotic inverse: SEP–**92**, 267–292.

Fowler, P., 1988, Seismic velocity estimation using prestack time migration: Ph.D. thesis, Stanford University.

Gradshtein, I. S., and Ryzhik, I. M., 1994, Table of integrals, series, and products: Boston: Academic Press.

Jakubowicz, H., and Levin, S., 1983, A simple exact method of three-dimensional migration – Theory: Geophys. Prosp., **31**, no. 1, 34–56.

Larner, K., and Beasley, C., 1987, Cascaded migrations—Improving the accuracy of finite-difference migration: Geophysics, **52**, no. 5, 618–643.

Levin, S., 1986a, Cascaded fifteen degree equations simplified: SEP–**48**, 101–108.

Levin, S., 1986b, Test your migration IQ: SEP–**48**, 147–160.

Li, Z., 1986, Cascaded one step fifteen degree migration versus Stolt migration: SEP–**48**, 85–100.

Liptow, F., and Hubral, P., 1995, Migrating around in circles: The Leading Edge, **14**, no. 11, 1125–1127.

Liu, Z., and Bleistein, N., 1995, Migration velocity analysis: Theory and iterative algorithm: Geophysics, **60**, no. 1, 142–153.

MacKay, S., and Abma, R., 1992, Imaging and velocity estimation with depth-focusing analysis: Geophysics, **57**, no. 12, 1608–1622.

Popovici, A. M., 1995, Prestack migration by split-step DSR: SEP–**84**, 53–60.

Rothman, D. H., Levin, S. A., and Rocca, F., 1985, Residual migration – applications and limitations: Geophysics, **50**, no. 1, 110–126.

Schneider, W. A., 1978, Integral formulation for migration in two-dimensions and three-dimensions: Geophysics, **43**, no. 1, 49–76.

Stolt, R. H., 1978, Migration by Fourier transform: Geophysics, **43**, no. 1, 23–48.

Tygel, M., Schleicher, J., and Hubral, P., 1994, Pulse distortion in depth migration: Geophysics, **59**, no. 10, 1561–1569.

Yilmaz, O., and Chambers, R. E., 1984, Migration velocity analysis by wave-field extrapolation: Geophysics, **49**, no. 10, 1664–1674.

Yilmaz, O., and Claerbout, J. F., 1980, Prestack partial migration: Geophysics, **45**, no. 12, 1753–1779.

Yilmaz, O., 1979, Prestack partial migration: Ph.D. thesis, Stanford University.

APPENDIX A

DERIVING THE KINEMATIC EQUATIONS

The main goal of this appendix is to derive the partial differential equation describing the image surface in a depth-midpoint-offset-velocity space.

The derivation starts with observing a simple geometry of reflection in a constant-velocity medium, shown in Figure A-1. The well-known equations for the apparent slowness

$$\frac{\partial t}{\partial s} = \frac{\sin\alpha_1}{v}\,, \tag{A-1}$$

$$\frac{\partial t}{\partial r} = \frac{\sin\alpha_2}{v} \tag{A-2}$$

relate the first-order traveltime derivatives for the reflected waves to the emergency angles of the incident and reflected rays. Here s stands for the source location at the surface, r is the receiver location, t is the reflection traveltime, v is the constant velocity, and α_1 and α_2 are the

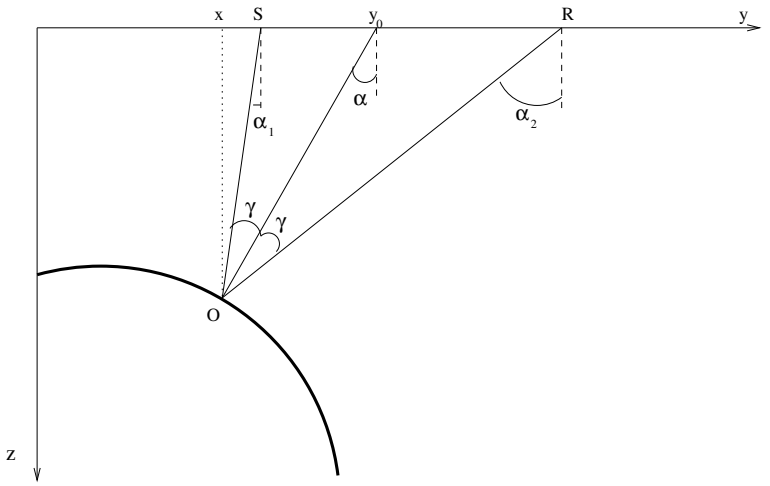

Figure A-1: Reflection rays in a constant velocity medium (a scheme). velcon1-vlcray [NR]

angles shown in Figure A-1. Considering the traveltime derivative with respect to the depth of the observation surface z, we can see that the contributions of the two branches of the reflected ray, added together, form the equation

$$-\frac{\partial t}{\partial z} = \frac{\cos\alpha_1}{v} + \frac{\cos\alpha_2}{v} \,. \tag{A-3}$$

It is worth mentioning that the elimination of angles from equations (A-1), (A-2), and (A-3) leads to the famous *double-square-root equation,*

$$-v\,\frac{\partial t}{\partial z} = \sqrt{1 - v^2 \left(\frac{\partial t}{\partial s}\right)^2} + \sqrt{1 - v^2 \left(\frac{\partial t}{\partial r}\right)^2} \,, \tag{A-4}$$

published in the Russian literature by Belonosova and Alekseev (1967) and commonly used in the form of a pseudo-differential dispersion relation (Clayton, 1978; Claerbout, 1985) for prestack migration (Yilmaz, 1979; Popovici, 1995). Considered locally, equation (A-4) is independent of the constant velocity assumption and enables prestack downward continuation of reflected waves in heterogeneous media.

Introducing midpoint coordinate $x = \frac{s+r}{2}$ and half-offset $h = \frac{r-s}{2}$, we can apply the chain rule and elementary trigonometric equalities to formulas (A-1) and (A-2) and transform these formulas to

$$\frac{\partial t}{\partial x} = \frac{\partial t}{\partial s} + \frac{\partial t}{\partial r} = \frac{2\sin\alpha\,\cos\gamma}{v} \,, \tag{A-5}$$

$$\frac{\partial t}{\partial h} = \frac{\partial t}{\partial r} - \frac{\partial t}{\partial s} = \frac{2\cos\alpha\,\sin\gamma}{v} \,, \tag{A-6}$$

where $\alpha = \frac{\alpha_1+\alpha_2}{2}$ is the dip angle, and $\gamma = \frac{\alpha_2-\alpha_1}{2}$ is the reflection angle (Clayton, 1978; Claerbout, 1985). Equation (A-3) transforms analogously to

$$-\frac{\partial t}{\partial z} = \frac{2\cos\alpha\,\cos\gamma}{v} \,. \tag{A-7}$$

This form of equation (A-3) is used to describe the stretching factor of the waveform distortion in depth migration (Tygel et al., 1994).

Dividing (A-5) and (A-6) by (A-7), we obtain

$$\frac{\partial z}{\partial x} = -\tan\alpha \,, \tag{A-8}$$

$$\frac{\partial z}{\partial h} = -\tan\gamma \,. \tag{A-9}$$

Substituting formulas (A-8) and (A-9) into equation (A-7) yields yet another form of the double-square-root equation:

$$-\frac{\partial t}{\partial z} = \frac{2}{v}\sqrt{1+\left(\frac{\partial z}{\partial x}\right)^2}\sqrt{1+\left(\frac{\partial z}{\partial h}\right)^2}, \tag{A-10}$$

which is analogous to the dispersion relationship of Stolt prestack migration (Stolt, 1978).

The law of sines in the triangle formed by the incident and reflected ray leads to the explicit relationship between the traveltime and the offset:

$$v\,t = 2h\,\frac{\cos\alpha_1+\cos\alpha_2}{\sin(\alpha_2-\alpha_1)} = 2h\,\frac{\cos\alpha}{\sin\gamma} \,. \tag{A-11}$$

The combination of formulas (A-11), (A-5), and (A-6) forms the basic kinematic equation of the offset continuation theory (Fomel, 1995):

$$\frac{\partial t}{\partial h}\left(t^2+\frac{4h^2}{v^2}\right) = h\,t\left(\frac{4}{v^2}+\left(\frac{\partial t}{\partial h}\right)^2-\left(\frac{\partial t}{\partial x}\right)^2\right) . \tag{A-12}$$

Differentiating (A-11) with respect to the velocity v yields

$$-v^2\,\frac{\partial t}{\partial v} = 2h\,\frac{\cos\alpha}{\sin\gamma} \,. \tag{A-13}$$

Finally, dividing (A-13) by (A-7), we get

$$v\,\frac{\partial z}{\partial v} = \frac{h}{\cos\gamma\,\sin\gamma} \,. \tag{A-14}$$

Equation (A-14) can be written in a variety of ways with the help of an explicit geometric relationship between the half-offset h and the depth z,

$$h = z\,\frac{\sin\gamma\,\cos\gamma}{\cos^2\alpha-\sin^2\gamma} \,, \tag{A-15}$$

which follows directly from the trigonometry of the triangle in Figure A-1 (Fomel, 1995). For example, equation (A-14) can be transformed to the form obtained recently by Liu and Bleistein (1995):

$$v\,\frac{\partial z}{\partial v} = \frac{z}{\cos^2\alpha-\sin^2\gamma} = \frac{z}{\cos\alpha_1\,\cos\alpha_2} \,. \tag{A-16}$$

In order to separate different factors contributing to the velocity continuation process, we can transform this equation to the form

$$v\,\frac{\partial z}{\partial v} = \frac{z}{\cos^2\alpha} + \frac{h^2}{z}\left(1-\tan^2\alpha\,\tan^2\gamma\right) =$$

$$= z\left(1+\left(\frac{\partial z}{\partial x}\right)^2\right) + \frac{h^2}{z}\left(1-\left(\frac{\partial z}{\partial x}\right)^2\left(\frac{\partial z}{\partial h}\right)^2\right) . \tag{A-17}$$

Rewritten in terms of the vertical traveltime, it further transforms to equation (1) in the main text. Yet another form of the kinematic velocity continuation equation follows from eliminating the reflection angle γ from equations (A-14) and (A-15). The resultant expression takes the following form:

$$v\,\frac{\partial z}{\partial v} = \frac{2\,(z^2+h^2)}{\sqrt{z^2+h^2\sin^2 2\alpha}+z\cos 2\alpha} = \frac{z}{\cos^2\alpha} + \frac{2\,h^2}{\sqrt{z^2+h^2\sin^2 2\alpha}+z} . \tag{A-18}$$

APPENDIX B

INTEGRAL VELOCITY CONTINUATION AND KIRCHHOFF MIGRATION

The goal of this appendix is to prove the equivalence between the result of the zero-offset velocity continuation from zero velocity and the conventional post-stack migration. After solving the velocity continuation problem in the frequency domain, I transform the solution back to the time-and-space domain and compare it with the famous Kirchhoff migration operator.

Zero-offset migration based on velocity continuation is the solution of the boundary problem for equation (55) with the boundary condition

$$P|_{v=0} = P_0 , \tag{B-1}$$

where $P_0(t_0,x_0)$ is the zero-offset seismic section, and $P(t,x,v)$ is the continued wavefield. In order to find the solution of the boundary problem composed of (55) and (B-1), it is convenient to apply the function transformation $R(t,x,v) = t\,P(t,x,v)$, the time coordinate transformation $\sigma = t^2/2$, and, finally, the double Fourier transform over the squared time coordinate σ and the spatial coordinate x:

$$\widehat{R}(v) = \int\int P(t,x,v)\exp(i\Omega\sigma - ikx)\,t^2\,dt\,dx . \tag{B-2}$$

With the change of domain, equation (55) transforms to the ordinary differential equation

$$\frac{d\,\widehat{R}}{d\,v} = i\,\frac{k^2}{\Omega}\,v\,\widehat{R} , \tag{B-3}$$

and the boundary condition (B-1) transforms to the initial value condition

$$\widehat{R}(0) = \widehat{R}_0 \,, \tag{B-4}$$

where

$$\widehat{R}_0 = \int\int P_0(t_0, x_0) \exp(i\,\Omega\sigma_0 - i\,k\,x_0)\, t_0^2\, dt_0\, dx_0 \,, \tag{B-5}$$

and $\sigma_0 = t_0^2/2$. The unique solution of the initial value (Cauchy) problem (B-3) - (B-4) is easily found to be

$$\widehat{R}(v) = \widehat{R}_0 \exp\left(i\,\frac{k^2}{2\,\Omega}\, v^2 \right) . \tag{B-6}$$

We can see that, in the transformed domain, velocity continuation is a unitary phase-shift operator. An immediate consequence of this remarkable fact is the cascaded migration decomposition of post-stack migration (Larner and Beasley, 1987):

$$\exp\left(i\,\frac{k^2}{2\,\Omega}\,(v_1^2 + \cdots + v_n^2) \right) = \exp\left(i\,\frac{k^2}{2\,\Omega}\, v_1^2 \right) \cdots \exp\left(i\,\frac{k^2}{2\,\Omega}\, v_n^2 \right) . \tag{B-7}$$

Analogously, three-dimensional post-stack migration is decomposed into the two-pass procedure (Jakubowicz and Levin, 1983):

$$\exp\left(i\,\frac{k_1^2 + k_2^2}{2\,\Omega}\, v^2 \right) = \exp\left(i\,\frac{k_1^2}{2\,\Omega}\, v^2 \right) \exp\left(i\,\frac{k_2^2}{2\,\Omega}\, v^2 \right) . \tag{B-8}$$

The inverse double Fourier transform of both sides of equality (B-6) yields the integral (convolution) operator

$$P(t, x, v) = \int\int P_0(t_0, x_0)\, K(t_0, x_0; t, x, v)\, dt_0\, dx_0 \,, \tag{B-9}$$

with the kernel K defined by

$$K = \frac{t_0^2/t}{(2\,\pi)^{m+1}} \int\int \exp\left(i\,\frac{k^2}{2\,\Omega}\, v^2 + i\,k\,(x - x_0) - \frac{i\,\Omega}{2}\,(t^2 - t_0^2) \right) dk\, d\Omega \,, \tag{B-10}$$

where m is the number of dimensions in x and k (m equals 1 or 2). The inner integral on the wavenumber axis k in formula (B-10) is a known table integral (Gradshtein and Ryzhik, 1994). Evaluating this integral simplifies equation (B-10) to the form

$$K = \frac{t_0^2/t}{(2\,\pi)^{m/2+1}\, v^m} \int (i\,\Omega)^{m/2} \exp\left[\frac{i\,\Omega}{2} \left(t_0^2 - t^2 - \frac{(x - x_0)^2}{v^2} \right) \right] d\Omega \,. \tag{B-11}$$

The term $(i\,\Omega)^{m/2}$ is the spectrum of the anti-causal derivative operator $\frac{d}{d\sigma}$ of the order $m/2$. Noting the equivalence

$$\left(\frac{\partial}{\partial\sigma} \right)^{m/2} = \left(\frac{1}{t}\,\frac{\partial}{\partial t} \right)^{m/2} = \left(\frac{1}{t} \right)^{m/2} \left(\frac{\partial}{\partial t} \right)^{m/2} \,, \tag{B-12}$$

which is exact in the 3-D case ($m = 2$) and asymptotically correct in the 2-D case ($m = 1$), and applying the convolution theorem, we can transform operator (B-9) to the form

$$P(t,x,v) = \frac{1}{(2\pi)^{m/2}} \int \frac{\cos\alpha}{(v\,\rho)^{m/2}} \left(-\frac{\partial}{\partial t_0}\right)^{m/2} P_0\left(\frac{\rho}{v}, x_0\right) dx_0 \,, \tag{B-13}$$

where $\rho = \sqrt{v^2 t^2 + (x - x_0)^2}$, and $\cos\alpha = t_0/t$. Operator (B-13) coincides with the Kirchhoff operator of the conventional post-stack time migration (Schneider, 1978).

APPENDIX C

FINITE-DIFFERENCING POST-STACK VELOCITY CONTINUATION

The differential equation (55), with the first-order derivative term neglected, has the mathematical form almost similar to the 15-degree wave extrapolation equation. Its finite-difference implementation, first described by Claerbout (1986) and Li (1986), is analogous to that of the 15-degree equation (Claerbout, 1976), except for the variant coefficients. We can write the implicit unconditionally stable finite-difference scheme for the velocity continuation equation in the form

$$(\mathbf{I} + a^{i+1}_{j+1}\,\mathbf{T})\,\mathbf{P}^{i+1}_{j+1} - (\mathbf{I} - a^{i+1}_{j}\,\mathbf{T})\,\mathbf{P}^{i+1}_{j} - (\mathbf{I} - a^{i}_{j+1}\,\mathbf{T})\,\mathbf{P}^{i}_{j+1} + (\mathbf{I} + a^{i}_{j}\,\mathbf{T})\,\mathbf{P}^{i}_{j} = 0 \,, \tag{C-1}$$

where index i corresponds to the time dimension, index j corresponds to the velocity dimension, $\mathbf{P}$ is a vector along the midpoint direction, $\mathbf{I}$ is the identity matrix, $\mathbf{T}$ represents the second-derivative operator in midpoint, and the coefficient a has the expression

$$a^i_j = v_j\, t_i\, \frac{\Delta v\, \Delta t}{(\Delta x)^2} \,. \tag{C-2}$$

In the two-dimensional case, equation (C-1) reduces to a tridiagonal system of linear equations, which can be easily inverted. The direction of stable propagation is either forward in velocity and backward in time or backward in velocity and forward in time as shown in Figure C-1.

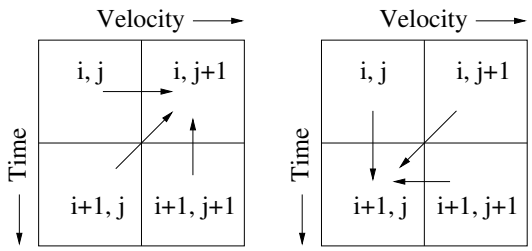

Figure C-1: Finite-difference scheme for the velocity continuation equation. A stable propagation is either forward in velocity and backward in time (left plot) or backward in velocity and forward in time (right plot). velcon1-vlcfds [NR]

The following simple ratfor program implements the finite-difference velocity continuation. It is slightly modified from Jon Claerbout's original version and has a more straightforward loop structure than Zhiming Li's `Caso15` program.

```
module velconx {
  use diffxx2
  use tridiag
  real, dimension (nx), allocatable       :: r, ld, rd, rhs
  real, dimension (:,:), pointer, private :: pt
  real                                    :: v1, v2, t0, dt
  real,                           private :: dv, a0
  real, parameter,                private :: b = 0.122996
  integer                                 :: nt, nx, nv, inv
#% _init (inv, v1,v2,t0, nt,nx,nv, dt,dx)
    real,    intent (in) :: dx
    allocate (pt(nt,nx))
    dv = (v1-v2)/nv; a0=(4.*dx*dx)/(dt*dv)
    call rtris_init (nx)
#% _lop (p1 (nt,nx), p2 (nt,nx))
    integer                     :: iv1, iv2, ivs, iv
    integer                     :: it1, it2, its, it
    real                        :: v, t, a, b1, b2, offd, diag
    real, dimension (:), pointer :: l
    if (adj) {
       iv1=1;  iv2=nv; ivs= 1
       it1=nt; it2= 2; its=-1; pt = p2
    } else {
       iv1=nv; iv2= 1; ivs=-1
       it1= 2; it2=nt; its= 1; pt = p1
    }
    do iv=iv1,iv2,ivs {  v=sqrt(v2+(iv-0.5)*dv); rhs = 0.
    do it=it1,it2,its {  t=t0+dt*(it-1)
          select case (inv) {
          case (0)
             t=sqrt(t)*v;       a=a0/t          ! Pseudounitary
          case(1)
             t=t*v;             a=a0/v          ! Claerbout's
          case default
             a=a0/(t*v);        t=v             ! True-amplitude
          }
          b1=b*a+t; b2=b*a-t; offd=a-b2; diag=a-2*b2
          l => pt(it,:);                         call diffxx(l,ld)
          rhs = rhs + a*l + b1*ld
          call tris(offd,b2,diag,b2,offd,rhs,r); call diffxx(r,rd)
          rhs = a*r + b1*rd - a*l - b2*ld ; l = r
    }}
    if (adj)
       p1 = p1 + pt
    else
       p2 = p2 + pt
#% _close
    deallocate (pt)
    call rtris_close ()
}
```

The parameter `adj` controls the direction of propagation. It is equal to zero for backward propagation, which corresponds to the modeling (demigration) operator. The parameter `inv` controls the amplitude behavior by introducing time-dependent divisors to equation (C-1).

For `inv=1`, the program implements Claerbout's velocity continuation equation. For `inv=2`, it implements the modified equation (55). The value of `inv=0` corresponds to the intermediate case. It leads to the *pseudounitary* velocity continuation, for which the reverse continuation is the exact adjoint operator (Fomel, 1996). We can easily test different types of amplitude behavior with the dot-product test and its modifications. The parameter `b` is required for the "1/6 trick" introduced by Claerbout (1985) to increase the accuracy of the second-derivative operator **T** in (C-1). The second-order difference in subroutine `diffxx` implies simple zero-slope boundary conditions on the midpoint coordinate. The call to `rtris` solves the triadiagonal system.

In order to test the performance of the finite-difference velocity continuation method, I use a simple synthetic model from **Basic Earth Imaging** (Claerbout, 1995). The "reflectivity" model is shown in Figure C-2. It contains several features challenging the migration performance: dipping beds, unconformity, syncline, anticline, and fault.

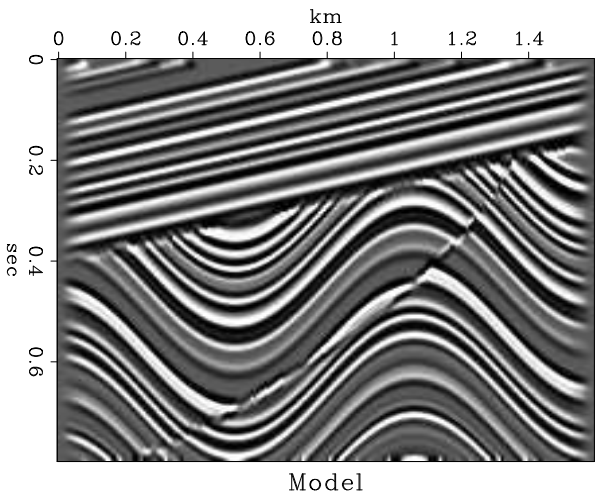

Figure C-2: Synthetic model for testing finite-difference migration by velocity continuation. velcon1-vlcmod [ER]

The following series of figures compares invertability of different migration methods. In all cases, constant-velocity modeling (demigration) by the adjoint operator was followed by migration with the correct velocity v=1500 m/sec. Figures C-3, C-4, C-5, C-6 show the results of modeling and migration with fast (nearest-neighbor) Kirchhoff, antialiased Kirchhoff (Fomel and Biondi, 1995), phase-shift (Gazdag), and Stolt methods respectively. These figures should be compared with Figure C-7, showing the analogous result of the finite-difference velocity continuation. The comparison reveals a remarkable invertability of velocity continuation, which reconstructs accurately the main features and frequency content of the model. Since the forward operators were different for different migrations, this comparison did not test the migration properties themselves. For such a test, I compare the results of the phase-shift and velocity-continuation migrations after Stolt modeling. The result of velocity continuation, shown in Figure C-8 is at least as accurate as that of the phase-shift method.

We can conclude that finite-difference velocity continuation is an attractive migration method. It possesses remarkable invertability properties, which might be useful in some applications. According to Li (1986), the computational speed of this method compares favorably with that of Stolt migration. The advantage is apparent for cascaded migration or migration

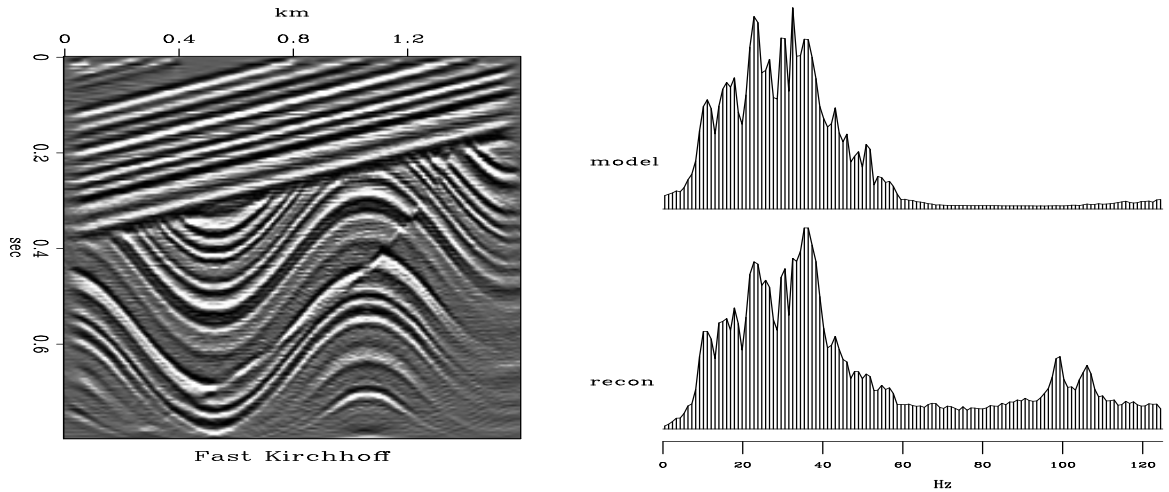

Figure C-3: Result of modeling and migration with the fast Kirchhoff method. Left plot shows the reconstructed model. Right plot compares the average amplitude spectrum of the true model with that of the reconstructed image. velcon1-vlckir [ER]

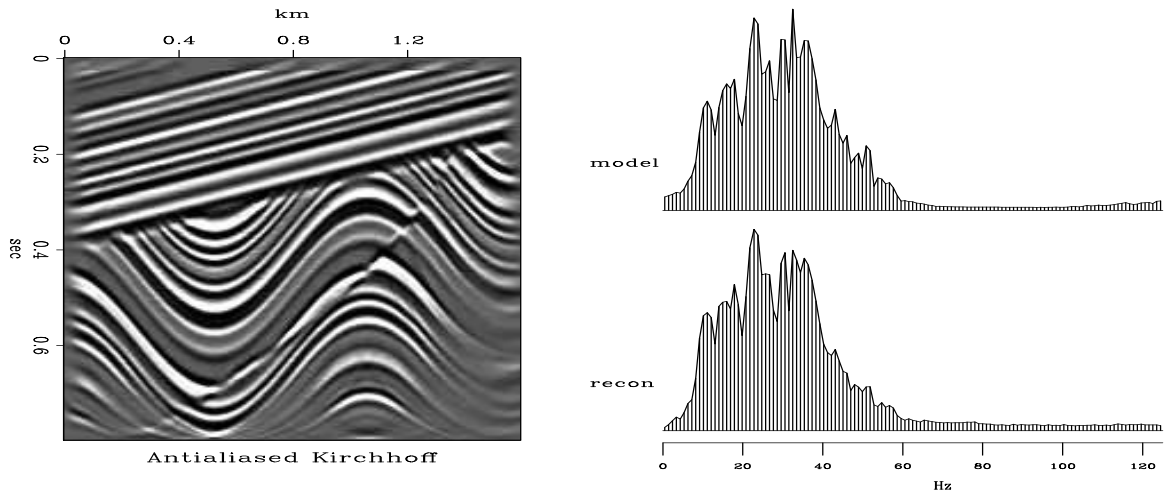

Figure C-4: Result of modeling and migration with the antialiased Kirchhoff method. Left plot shows the reconstructed model. Right plot compares the average amplitude spectrum of the true model with that of the reconstructed image. velcon1-vlckaa [ER]

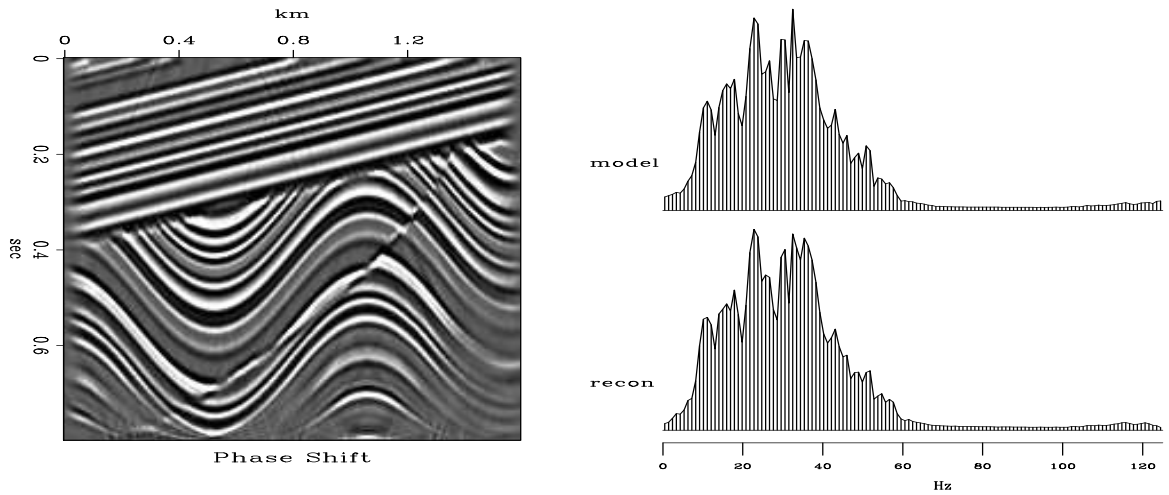

Figure C-5: Result of modeling and migration with the phase-shift method. Left plot shows the reconstructed model. Right plot compares the average amplitude spectrum of the true model with that of the reconstructed image. velcon1-vlcpha [ER]

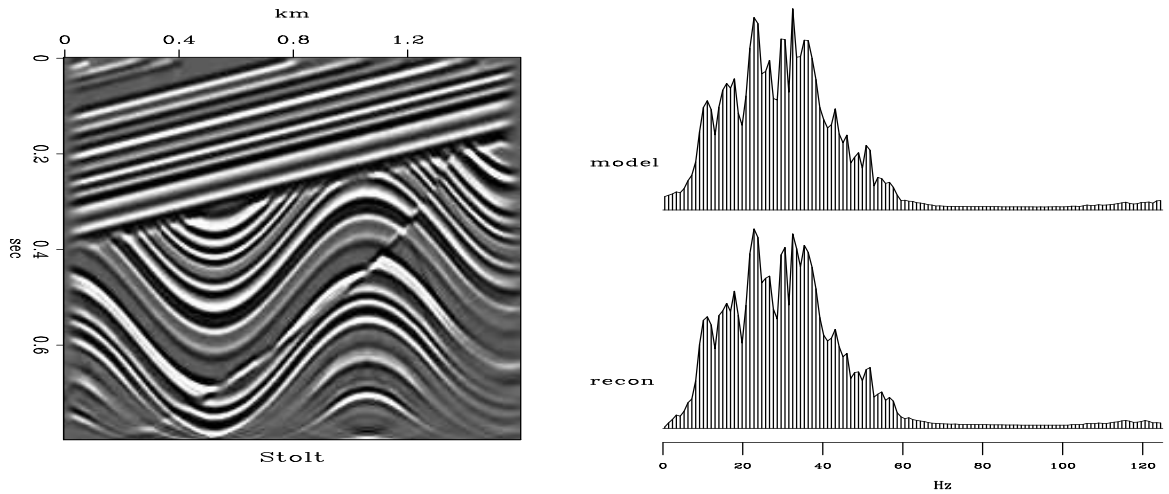

Figure C-6: Result of modeling and migration with Stolt method. Left plot shows the reconstructed model. Right plot compares the average amplitude spectrum of the true model with that of the reconstructed image. velcon1-vlcsto [ER]

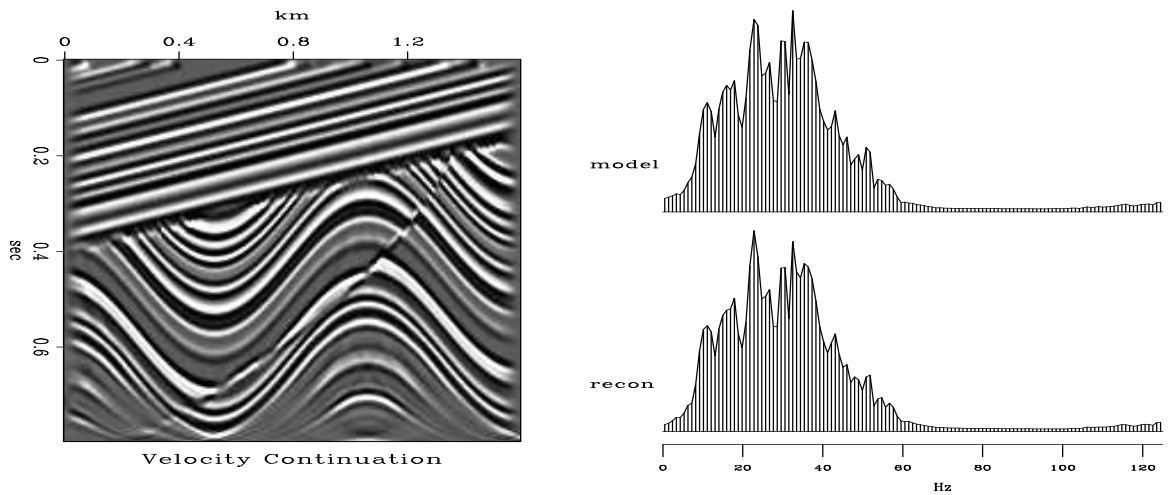

Figure C-7: Result of modeling and migration with the finite-difference velocity continuation. Left plot shows the reconstructed model. Right plot compares the average amplitude spectrum of the true model with that of the reconstructed image. velcon1-vlcvel [ER]

with multiple velocity models. In these cases, the cost of Stolt migration increases in direct proportion with the number of velocity models, while the cost of velocity continuation stays the same.

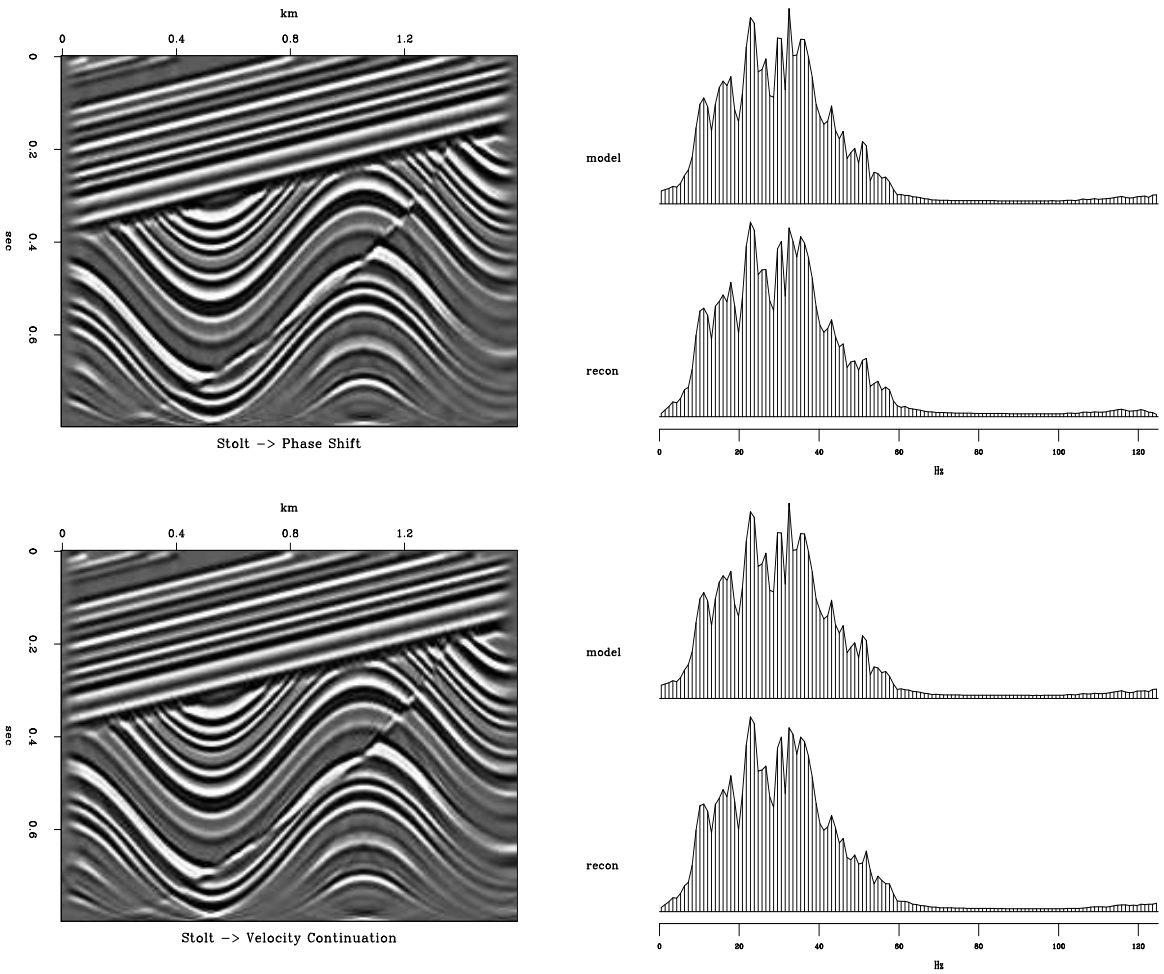

Figure C-8: Top plot: modeling with Stolt method, migration with the phase-shift method. Bottom plot: modeling with Stolt method, migration with the finite-difference velocity continuation. Left plots show the reconstructed models. Right plots compare the average amplitude spectrum of the true model with that of the reconstructed image. velcon1-vlcspv [ER]